Synthesis, Characterization, and Reversible Oxygenation of μ-Alkoxo Diiron(II) Complexes with the Dinucleating Ligand *N,N,N′,N′*-Tetrakis{(6-methyl-2-pyridyl)methyl}-1,3-diaminopropan-2-olate†

Yoshihito Hayashi,[1] Takayuki Kayatani,[1] Hideki Sugimoto,[1] Masatatsu Suzuki,*[,1] Katsuhiko Inomata,[1] Akira Uehara,*[,1] Yasuhisa Mizutani,[2] Teizo Kitagawa,*[,2] and Yonezo Maeda[3]

Contribution from the Department of Chemistry, Faculty of Science, Kanazawa University, Kakuma-machi, Kanazawa 920-11, Japan, Institute for Molecular Science, Okazaki 444, Japan, and Department of Chemistry, Faculty of Science, Kyushu University, Hakozaki, Higasiku, Fukuoka 812, Japan

Received November 14, 1994[⊗]

Abstract: Two new types of dinucleating ligands, symmetric Me_4-tpdp and asymmetric Me_2-tpdp, were synthesized (Me_4-tpdp = *N,N,N′,N′*-tetrakis{(6-methyl-2-pyridyl)methyl}-1,3-diaminopropan-2-olate and Me_2-tpdp = *N,N*-bis-{(6-methyl-2-pyridyl)methyl}-*N′,N′*-bis(2-pyridylmethyl)-1,3-diaminopropan-2-olate). Their μ-alkoxo diiron(II) complexes $[Fe_2(Me_4\text{-tpdp})(C_6H_5COO)(H_2O)](BF_4)_2$ (**1**), $[Fe_2(Me_4\text{-tpdp})(CF_3CO_2)(H_2O)_2](BF_4)_2 \cdot H_2O$ (**2**), and $[Fe_2(Me_2\text{-tpdp})(CF_3CO_2)](BF_4)_2 \cdot nH_2O$ (**3**) were synthesized, and the structure of complex **1** was determined by X-ray crystallography. Complex **1** crystallizes in the monoclinic space group $P2_1/n$ with a = 19.257(2) Å, b = 17.166(3) Å, c = 12.558(2) Å, β = 96.55(1)°, and Z = 4. The complex has a doubly bridged structure with a μ-alkoxo of Me_4-tpdp and μ-benzoate and contains two distinct iron centers: one five-coordinate iron center with an N_3O_2 donor set and one six-coordinate iron center with an N_3O_3 donor set with an additional coordinated water molecule. Introduction of a 6-methyl group in the pyridyl group results in elongation of the Fe−N(pyridyl) bond distances. The Fe−N and Fe−O bond distances in the six-coordinate iron center are substantially longer than those in the five-coordinate iron center except for the Fe−N(tertiary amine) bonds. The Mössbauer spectrum of **1** exhibited two sets of quadrupole doublets corresponding to the two distinct iron centers. The electronic spectra of **1** revealed that dissociation of the coordinated water occurs in CH_2Cl_2 to form two five-coordinate iron centers, whereas in DMSO, six-coordinate iron centers are predominant due to the coordination of DMSO. Complexes **1** and **2** showed reversible oxygenation at −40 °C, whereas reversible oxygenation was not observed for complex **3**. The thermal stability of the oxy complexes toward irreversible oxidation is highly dependent on the relative degree of steric bulkiness of the dinucleating ligands and their electron donor ability; introduction of the 6-methyl group in the pyridyl group stabilizes the oxy form toward irreversible oxidation. The resonance Raman spectrum of the oxy-**1** exhibited two oxygen-isotope sensitive bands in the ν(O−O) region and two bands in the ν(Fe−O) region. The presence of the two ν(O−O) Raman bands at 918 and 891 cm^{-1} is interpreted in terms of Fermi resonance, while the two ν(Fe−O) bands are assigned to the symmetric and antisymmetric combinations of Fe−O stretchings of the Fe−O−O−Fe unit. Thus the Raman spectra indicated the formation of the μ-peroxo species. The oxygen affinities ($P_{1/2}$) of the complexes were determined for the first time by spectrophotometric methods; those of **1** and **2** in CH_2Cl_2 at −40 °C are ca. 6 and ca. 41 Torr, respectively.

Introduction

Dinuclear iron complexes have been of particular interest as models of hemerythrin (Hr), ribonucleotide reductase (RRB2), and methane monooxygenase (MMO).[4-11] Hr binds O_2 reversibly in a hydroperoxo form, while RRB2 and MMO activate O_2 to oxidize tyrosine to a tyrosine radical and to hydroxylate methane to methanol, respectively.

A variety of diiron(III) complexes has been reported as structural and spectroscopic models for the inactive forms of the above dinuclear iron proteins,[12,13] whereas only a limited

† This paper is dedicated to the late Professor Nobumasa Kitajima.

⊗ Abstract published in *Advance ACS Abstracts*, November 1, 1995.

(1) Kanazawa University.

(2) Institute for Molecular Science.

(3) Kyushu University.

(4) (a) Kurtz, D. M., Jr.; Shriver, D. F.; Kolz, I. M. *Coord. Chem. Rev.* **1977**, 145−178. (b) Willkins, R. G.; Harrington, P. C. *Adv. Inorg. Chem.* **1983**, *5*, 51−85. (c) Kolz, I. M.; Kurtz, D. M., Jr. *Acc. Chem. Res.* **1984**, *17*, 16−22. (d) Wilkins, P. C.; Wilkins, R. G. *Coord. Chem. Rev.* **1987**, *79*, 195−214. (e) Stenkamp, R. E. *Chem. Rev.* **1994**, *94*, 715−726.

(5) (a) Sjöberg, B.-M.; Gräslund, A. *Adv. Inorg. Chem.* **1983**, *5*, 87−110. (b) Nordlund, P.; Sjöberg, B.-M.; Eklund, H. *Nature* **1990**, *345*, 593−598. (c) Bollinger, J. M., Jr.; Edmondson, D. E.; Huynh, B. H.; Filley, J.; Norton, J. R.; Stubbe, J. *Science* **1991**, *253*, 292−298.

(6) (a) DeWitt, J. G.; Bentsen, J. G.; Rosenzweig, A. C.; Hedman, B.; Green, J.; Pilkington, S.; Papaefthymiou, G. C.; Dalton, H.; Hodgson, K. O.; Lippard, S. J. *J. Am. Chem. Soc.* **1991**, *113*, 9219−9235. (b) Liu, K. E.; Johnson, C. C.; Newcomb, M.; Lippard, S. J. *J. Am. Chem. Soc.* **1993**, *115*, 939−947. (c) Rosenzweig, A. C.; Frederick, C. A.; Lippard, S. J.; Nordlund, P. *Nature* **1993**, *366*, 537−543.

(7) Sanders-Loehr, J. In *Iron Carriers and Iron Proteins*; Loehr, T. M., Ed.; VCH Press: New York, 1989.

(8) Vincent, J. B.; Olivier-Lilley, G. L.; Averill, B. A. *Chem. Rev.* **1990**, *90*, 1447−1467.

(9) Que, L., Jr.; True, A. E. *Prog. Inorg. Chem.* **1990**, *38*, 97−200.

(10) Que, L., Jr. In *Bioinorganic Catalysis*; Reedijk, J., Ed.; Marcel Dekker Inc.: Amsterdam, 1993; pp 347−393.

(11) Feig, A. L.; Lippard, S. J. *Chem. Rev.* **1994**, *94*, 759−805.

(12) Lippard, S. J. *Angew. Chem., Int. Ed. Engl.* **1988**, *27*, 344−361 and references cited therein.

0002-7863/95/1517-11220$09.00/0

number of diiron(II) complexes have been reported.[14-19] The chemistry of dinuclear iron complexes are of particular importance to gain insight into the structures and functions of the active forms of the above proteins, especially with respect to the reversible binding and the activation of dioxygen. Although there are several μ-peroxo diiron complexes generated by the reaction of iron(III) complexes with hydrogen peroxide,[20] only a few iron(II) complexes which bind O_2 in a μ-peroxo form have been known.[21-23] Kitajima et al.[21] reported that the mononuclear iron(II) complex $[Fe\{HB(3,5\text{-}iPr_2Pz)_3\}(C_6H_5COO)]$[24] reversibly binds O_2 to form a μ-peroxo species at −20 °C. Que et al.[22] also reported that the dinuclear iron(II) complex of a dinucleating ligand, $[Fe_2(N\text{-Et-HPTB})(C_6H_5COO)]^{2+}$, forms a μ-peroxo species at −60 °C, whereas the oxygenation is irreversible.

Dinuclear metal complexes with sterically and electronically controlled environments are expected to bind O_2 reversibly in μ-peroxo form. We have demonstrated that dinuclear cobalt(II) complexes, $[Co_2(L)(RCOO)]^{2+}$, form μ-peroxo species and that their oxygen affinities and the thermal stability of μ-peroxo species toward the irreversible oxidation are highly dependent on the stereochemistry and the electron donor ability of the dinucleating ligands, where L represents a series of dinucleating ligands which have an N_6O donor set with a phenolate or alkoxide bridging group.[25] In our current studies on controlling the thermal stability of μ-peroxo complexes and the oxygen affinity of dimetal(II,II) complexes, we report, in this paper, the synthesis and characterization of the μ-alkoxo diiron(II) complexes of symmetric and asymmetric dinucleating ligands, Me_4-tpdp, Me_2-tpdp, and tpdp, and their oxygenation reactions. Preliminary results have been previously reported.[23]

Chart 1. Dinucleating Ligands

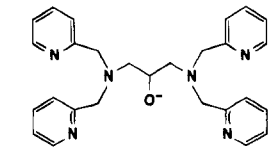

tpdp

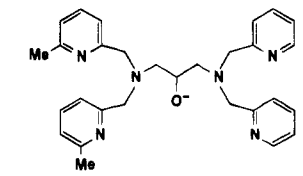

Me_2-tpdp

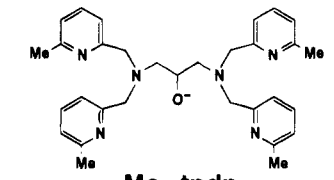

Me_4-tpdp

Experimental Section

Materials. Solvents for measurements were purified by refluxing with CaH_2 and distilled under Ar atmosphere. All other chemicals were of reagent grade.

Synthesis of Ligands. *N,N,N′,N′*-Tetrakis{(6-methyl-2-pyridyl)methyl}-1,3-diaminopropan-2-ol (Me_4-Htpdp). 1,3-Diamino-2-propanol dihydrochloride (4.9 g, 30 mmol) was dissolved in a small amount of water, to which was added 6-methyl-2-pyridinecarbaldehyde (15.7 g, 130 mmol) in 200 cm^3 of methanol. To the resulting solution was added sodium cyanotrihydridoborate (6.1 g, 97 mmol) dropwise with stirring. The solution was then stirred for 3 days at room temperature, subsequently acidified by addition of concentrated hydrochloric acid, and evaporated almost to dryness under reduced pressure. The residue was dissolved in 100 cm^3 of 0.1 mol dm^{-3} NaOH solution and extracted with three 50-cm^3 portions of chloroform. The combined extracts were dried over Na_2SO_4 and evaporated under reduced pressure to give an oily product, which was then purified by silica gel column chromatography with chloroform/methanol. Yield: 10.0 g (65%). ^1H NMR ($CDCl_3$, 400 MHz): δ = 2.50 (12H, s, CH_3), 2.56−2.70 (4H, m, CH_2), 3.83 (8H, m, CH_2py), 3.96 (1H, m, CH), 6.95 (4H, d, pyH), 7.18(4H, d, pyH), 7.45 (4H, t, pyH). ^{13}C NMR ($CDCl_3$, 100 MHz): δ = 24.3 (CH_3), 59.2 (CH_2), 61.0 (NCH_2py), 67.4 (CH), 119.8 (py), 121.3 (py), 136.5 (py), 157.5 (py), 159.1 (py). MS: *m/z* 510 $[M]^+$.

(Phthalimidomethyl)oxirane (A). A mixture of potassium phthalimide (9.26 g, 50 mmol) and epichlorohydrin (30 cm^3) was refluxed for 5 h at 120 °C, and excess epichlorohydrin was removed under reduced pressure to give a yellowish white powder. The yellowish white powder was recrystallized from methanol (50 cm^3). Yield: 8.1 g (80%). ^1H NMR ($CDCl_3$, 400 MHz): δ = 2.69 (1H, dd, CH_2O), 2.81 (1H, t, CH_2O), 3.25 (1H, m, CHO), 3.82 (1H, dd, CH_2N), 3.96 (1H, dd, CH_2N), 7.74 (2H, m, Ph), 7.88 (2H, m, Ph). ^{13}C NMR ($CDCl_3$, 100 MHz): δ = 39.7 (CH_2), 46.2 (CH_2), 49.1 (CH), 123.5 (Ph), 132.0 (Ph), 134.2 (Ph), 168.0 (CO). MS: *m/z* 203 $[M]^+$.

(13) Kurtz, D. M., Jr. *Chem. Rev.* **1990**, *90*, 585−606 and references cited therein.

(14) (a) Chaudhuri, P.; Wieghardt, K.; Nuber, B.; Weiss, J. *Angew. Chem., Int. Ed. Engl.* **1985**, *24*, 778−779. (b) Hartman, J. R.; Rardin, R. L.; Chaudhuri, P.; Pohl, K.; Wieghardt, K.; Nuber, B.; Weiss, J.; Papaefthymiou, G. C.; Frankel, R. B.; Lippard, S. J. *J. Am. Chem. Soc.* **1987**, *109*, 7387−7396.

(15) (a) Tolman, W. B.; Bino, A.; Lippard, S. J. *J. Am. Chem. Soc.* **1989**, *111*, 8522−8523. (b) Tolman, W. B.; Liu, S.; Bentsen, J. G.; Lippard, S. J. *J. Am. Chem. Soc.* **1991**, *113*, 152−164.

(16) (a) Suzuki, M.; Uehara, A.; Oshio, H.; Endo, K.; Yanaga, M.; Kida, S.; Saito, K. *Bull. Chem. Soc. Jpn.* **1987**, *60*, 3547−3555. (b) Brovik, A. S.; Que, L., Jr. *J. Am. Chem. Soc.* **1988**, *110*, 2345−2347. (c) Brovik, A. S.; Hendrich, M. P.; Holman, T. R.; Münck, E.; Papaefthymiou, V.; Que, L., Jr. *J. Am. Chem. Soc.* **1990**, *112*, 6031−6038. (d) Snyder, B. S.; Patterson, G. S.; Abrahamson, A. J.; Holm, R. H. *J. Am. Chem. Soc.* **1989**, *111*, 5214−5223. (e) Stassinopoulos, A.; Schulte, G.; Papaefthymiou, G. C.; Caradonna, J. P. *J. Am. Chem. Soc.* **1991**, *113*, 8686−8697.

(17) Kitajima, N.; Tamura, N.; Tanaka, M.; Moro-oka, Y. *Inorg. Chem.* **1992**, *31*, 3342−3343.

(18) Hagen, K. S.; Lachicotte, R. *J. Am. Chem. Soc.* **1992**, *114*, 8741−8742.

(19) Ménage, S.; Zang, Y.; Hendrich, M. P.; Que, L., Jr. *J. Am. Chem. Soc.* **1992**, *114*, 7786−7792.

(20) (a) Nishida, Y.; Takeuchi, M.; Shimo, H.; Kida, S. *Inorg. Chim. Acta* **1984**, *96*, 115−119. (b) Murch, B. P.; Bradley, F. C.; Que, L., Jr. *J. Am. Chem. Soc.* **1986**, *108*, 5027−5028. (c) Nishida, Y.; Takeuchi, M. *Z. Naturforsch.* **1987**, *42B*, 52−54. (d) Micklitz, W.; Bott, S. G.; Bentsen, J. G.; Lippard, S. J. *J. Am. Chem. Soc.* **1989**, *111*, 372−374. (e) Sawyer, D. T.; McDowell, M. S.; Spencer, L.; Tsang, P. K. S. *Inorg. Chem.* **1989**, *28*, 1166−1170. (f) Brennan, B. A.; Chen, Q.; Juarez-Garcia, C.; True, A. E.; O'Connor, C. J.; Que, L., Jr. *Inorg. Chem.* **1991**, *30*, 1937−1943.

(21) (a) Kitajima, N.; Fukui, H.; Moro-oka, Y.; Mizutani, Y.; Kitagawa, T. *J. Am. Chem. Soc.* **1990**, *112*, 6402−6403. (b) Kitajima, N.; Tamura, N.; Amagai, H.; Fukui, H.; Moro-oka, Y.; Mizutani, Y.; Kitagawa, T.; Mathur, R.; Heerwegh, K.; Reed, C. A.; Randall, C. R.; Que, L., Jr.; Tatsumi, K. *J. Am. Chem. Soc.* **1994**, *116*, 9071−9085.

(22) (a) Ménage, S.; Brennan, B. A.; Juarez-Garcia, C.; Münck, E.; Que, L., Jr. *J. Am. Chem. Soc.* **1990**, *112*, 6423−6425. (b) Dong, Y.; Ménage, S.; Brennan, B. A.; Elgren, T. E.; Jang, H. G.; Pearce, L. L.; Que, L., Jr. *J. Am. Chem. Soc.* **1993**, *115*, 1851−1859.

(23) Hayashi, Y.; Suzuki, M.; Uehara, A.; Mizutani, Y.; Kitagawa, T. *Chem. Lett.* **1992**, 91−94.

(24) Abbreviations of ligands used: $HB(3,5\text{-}iPr_2Pz)_3$ = hydrotris(3,5-bis(isopropyl)pyrazolyl)borate; *N*-Et-HPTB = *N,N,N′,N′*-tetrakis{(1-ethyl-2-benzimidazolyl)methyl}-1,3-diaminopropan-2-olate; BIPhMe = bis(1-methyl-2-imidazolyl)phenylmethoxymethane; tpdp = *N,N,N′,N′*-tetrakis(2-pyridylmethyl)-1,3-diaminopropan-2-olate; TPA = tris{(6-methyl-2-pyridyl)methyl}amine; bpmp = 2,6-bis[(bis(2-pyridylmethyl)amino)methyl]-4-methylphenolate; BF = benzoyl formate; BPh_4 = tetraphenylborate; tpdb = *N,N,N′,N′*-tetrakis(2-pyridylmethyl)-1,4-diaminobutan-2-olate.

(25) (a) Suzuki, M.; Ueda, I.; Kanatomi, H.; Murase, I. *Chem. Lett.* **1983**, 185−188. (b) Suzuki, M.; Kanatomi, H.; Murase, I. *Bull. Chem. Soc. Jpn.* **1984**, *57*, 36−42. (c) Suzuki, M.; Sugisawa, T.; Uehara, A. *Bull. Chem. Soc. Jpn.* **1990**, *63*, 1115−1120. (d) Kayatani, K.; Hayashi, Y.; Suzuki, M.; Uehara, A. *Bull. Chem. Soc. Jpn.* **1994**, *67*, 2980−2989.

Scheme 1. Synthetic Route of Me_2-Htpdp

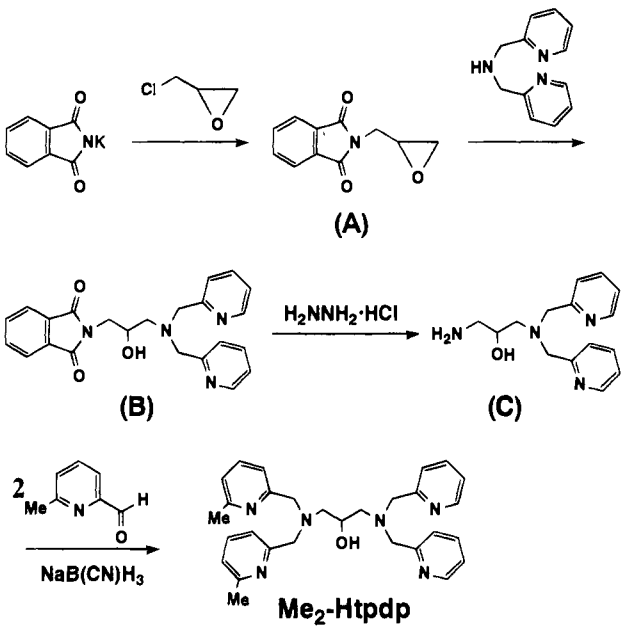

***N*-Phthaloyl-*N'*,*N'*-bis(2-pyridylmethyl)-1,3-diaminopropan-2-ol (B).** A mixture of **A** (8.13 g, 40 mmol) and bis(2-pyridylmethyl)-amine (7.97 g, 40 mmol) was heated for 3 h at 120 °C to give a black sticky product, which was subjected to silica gel column chromatography ($CHCl_3$/methanol) to obtain a brown oil. Yield: 10.5 g (65%). ^1H NMR ($CDCl_3$, 400 MHz): δ = 2.74 (1H, dd, CH_2N), 2.93 (1H, dd, CH_2N), 3.66 (1H, dd, CH_2N), 3.80 (1H, dd, CH_2N), 3.90 (2H, d, NCH_2-py), 3.97 (2H, d, NCH_2py), 4.16 (1H, m, CH), 7.09 (2H, m, py), 7.25 (2H, d, py), 7.54 (2H, dt, py), 7.69 (2H, dd, Ph), 7.82 (2H, dd, Ph), 8.48 (2H, m, py). ^{13}C NMR ($CDCl_3$, 100 MHz): δ = 41.9 (CH_2), 59.2 (CH_2), 60.5 (NCH_2py), 67.3 (CH), 122.0 (py), 123.0 (Ph), 123.2 (py), 132.1 (Ph), 133.8 (Ph), 136.4 (py), 148.9 (py), 159.1 (py), 168.4 (CO). MS: *m/z* 402 $[M]^+$.

***N*,*N*-Bis(2-pyridylmethyl)-1,3-diaminopropan-2ol (C).** A solution of **B** (10.5 g, 26 mmol) and hydrazine monohydrate (1.55 g, 31 mmol) in ethanol (50 cm^3) was refluxed for 3 h at 90 °C. The mixture was cooled to room temperature, followed by dropwise addition of diluted hydrochloric acid to acidify. After the mixture was heated for 30 min at 80 °C, the precipitate was filtered off. The filtrate was condensed almost to dryness under reduced pressure, and the residue was dissolved in water. The aqueous solution was made alkaline (pH ca. 10) by addition of Na_2CO_3. The oily layer separated off and was extracted with chloroform. The extract was dried over Na_2SO_4, and the solvent was removed under reduced pressure to give a brown oil which was subjected to silica gel column chromatography ($CHCl_3$/methanol) to obtain a brown oil. Yield: 6.5 g (67%). ^1H NMR ($CDCl_3$, 400 MHz): δ = 2.67 (4H, m, CH_2N), 3.37 (2H, br, NH_2), 3.80 (1H, m, CH), 3.87 (2H, d, NCH_2py), 3.95 (2H, d, NCH_2py), 7.13 (2H, dd, py), 7.35 (2H, d, py), 7.60 (2H, dt, py), 8.53 (2H, t, py). ^{13}C NMR ($CDCl_3$, 100 MHz): δ = 45.8 (CH_2), 58.9 (CH_2), 60.4 (NCH_2), 69.9 (CH), 122.1 (py), 123.1 (py), 136.5 (py), 149.0 (py), 159.1 (py). MS: *m/z* 272 $[M]^+$.

***N*,*N*-Bis{(6-methyl-2-pyridyl)methyl}-*N'*,*N'*-bis(2-pyridylmethyl)-1,3-diaminopropan-2-ol (Me_2-Htpdp).** This was prepared in a way similar to that of Me_4-Htpdp using **C**. A solution of **C** (5.45 g, 20 mmol) and concentrated HCl (3.4 mL, 40 mmol) in 50 mL of methanol was added to 6-methyl-2-pyridinecarbaldehyde (5.5 g, 45 mmol) in 100 cm^3 of methanol. The subsequent procedures are the same as those for Me_4-Htpdp. ^1H NMR ($CDCl_3$, 400 MHz): δ = 2.50 (6H, s, CH_3), 2.58−2.72 (4H, m, NCH_2), 3.84−3.88 (8H, m, NCH_2py), 3.91−4.01 (1H, m, CH), 6.96 (2H, d, py), 7.09(2H, m, py), 7.18 (2H, d, py), 7.38 (2H, d, py), 7.46 (2H, t, py), 7.57 (2H, m, py), 8.48 (2H, dd, py). ^{13}C NMR ($CDCl_3$, 100 MHz): δ = 24.3 (CH_3), 59.1 (CH_2), 59.2 (CH_2), 60.9 (CH_2), 64.0 (CH_2), 67.3 (CH), 119.9 (py), 121.4 (py), 121.9 (py), 123.1 (py), 136.3 (py), 136.6 (py), 148.9 (py), 157.6 (py), 158.9 (py), 159.6 (py). MS: *m/z* 482 $[M]^+$.

Tetrakis(2-pyridylmethyl)-1,3-diaminopropan-2-ol (Htpdp). This was prepared as described previously.[25c]

Synthesis of Complexes. All the manipulations for preparation of the diiron(II) complexes were carried out under Ar atmosphere using Schlenk techniques.

$[Fe_2(Me_4\text{-tpdp})(C_6H_5COO)(H_2O)](BF_4)_2$ (1). To a sitrred solution of 0.34 g (1.0 mmol) of $Fe(BF_4)_2{\cdot}6H_2O$ in 5 cm^3 of methanol was added a mixture of 0.26 g (0.5 mmol) of Me_4-Htpdp, 0.07 g (0.5 mmol) of C_6H_5COONa, and 0.03 g (0.5 mmol) of CH_3ONa in 10 cm^3 of methanol to form a dark yellow solution. After the solution was stirred for 1 h, the resulting solution was reduced in volume to 5 cm^3 by vacuum evaporation and then 10 cm^3 of water was added. The mixture was cooled in an ice bath for 15 min. Yellow microcrystals obtained were collected by filtration and washed with cold water. Recrystallization from methanol−water gave long needlelike crystals (0.31 g, 60%). Anal. Calcd for $C_{38}H_{44}N_6O_4Fe_2B_2F_8$: C, 48.86; H, 4.75; N, 9.00. Found: C, 48.95; H, 4.79; N, 9.02. IR (cm^{-1}): ν(OH), 3444; ν(C=C), 1605; ν_{as}(COO), 1560; ν_s(COO), 1396; $\nu_3(BF_4)$, 1074. ^1H NMR (CD_2Cl_2, 400 MHz, 300 K): δ = 182.9 (CH_2), 143.5 (CH), 124.1 (CH_2), 100.6 (CH_2), 72.0 (CH_2), 53.9 (*m*-py), 43.3 (*m*-py), 40.5 (*m*-py), 30.6 (*m*-py), 20.0 (CH_2), 17.1 (*o*-Ph), 16.4 (CH_3), 12.2 (*p*-Ph), 9.4 (*m*-Ph), −7.8 (*p*-py), −8.4 (*p*-py), −19.5 (CH_2), −46.3 (CH_3).

$[Fe_2(Me_4\text{-tpdp})(CF_3CO_2)(H_2O)_2](BF_4)_2{\cdot}H_2O$ (2). The complex was prepared in the same way as that for **1** except that CF_3COONa was used instead of C_6H_5COONa. Yellow microcrystalline materials were obtained. Yield: 58%. Anal. Calcd for $C_{33}H_{41}N_6O_5Fe_2B_2F_{11}$: C, 41.20; H, 4.51; N, 8.74. Found: C, 41.10; H, 4.48; N, 8.96. IR (cm^{-1}): ν(OH), 3448; ν_{as}(COO), 1684; ν(C=C), 1608; ν_s(COO), 1437; $\nu_3(BF_4)$, 1049. ^1H NMR (CD_2Cl_2, 400 MHz, 300 K): δ = 171.9 (CH_2), 126.2 (CH), 119.0 (CH_2), 95.6 (CH_2), 66.3 (CH_2), 53.4 (*m*-py), 41.7 (*m*-py), 40.1 (*m*-py), 31.7 (*m*-py), 14.1 (CH_3), 3.8 (CH_2), −7.1 (*p*-py), −9.2 (*p*-py), −36.8 (CH_3).

$[Fe_2(Me_2\text{-tpdp})(CF_3COO)](BF_4)_2{\cdot}nH_2O$ (3). The compound was prepared in the same way as that for **2** except that Me_2-Htpdp was used instead of Me_4-Htpdp. Yellow microcrystalline materials were obtained. Yield: 138 mg. The compound was air-sensitive and gave a brown compound when exposed to air. Elemental analysis of the brown compound was carried out. Anal. Calcd for $C_{31}H_{33}N_6O_3Fe_2B_2F_{11}{\cdot}O_2{\cdot}3H_2O$: C, 38.55; H, 4.07; N, 8.70. Found: C, 38.60; H, 3.97; N, 8.69. IR (cm^{-1}): ν(OH), 3430; ν_{as}(COO), 1674; ν(C=C), 1608; ν_s(COO), 1445; $\nu_3(BF_4)$, 1083.

$[Fe_2(tpdp)(C_6H_5COO)](BPh_4)_2{\cdot}H_2O$ (4). To an acetonitrile solution (20 cm^{-3}) containing 0.338 g (1.0 mmol) of $Fe(BF_4)_2{\cdot}6H_2O$ was added a mixture of Htpdp (0.227 g, 0.50 mmol), C_6H_5COOH (0.061 g, 0.50 mmol), and Et_3N (0.101 g, 1.0 mmol) in 10 cm^3 of methanol to form a dark yellow solution. After the solution was stirred for 1 h, a methanol solution (20 cm^3) of $NaBPh_4$ (0.513 g, 1.5 mmol) was added. The mixture was cooled in an ice bath to give microcrystals which were collected by filtration and washed with methanol and ether. Anal. Calcd for $C_{82}H_{76}N_6O_4Fe_2B_2$: C, 73.34; H, 5.70; N, 6.26. Found: C, 73.75; H, 5.70; N, 6.47.

$[Co_2(Me_2\text{-tpdp})(CH_3COO)](ClO_4)_2{\cdot}1.5H_2O{\cdot}0.25NaCl$ (5). To a solution of $Co(CH_3COO)_2{\cdot}4H_2O$ (0.25 g, 1.0 mmol) in 5 mL of ethanol was added an ethanol solution (5 mL) of Me_2-Htpdp (0.24 g, 0.50 mmol) with stirring. $NaClO_4$ (0.370 g, 3 mmol) dissolved in 3 mL of water was added to the above solution. The resulting purple solution was allowed to stand overnight at 0 °C to give pink crystals which were collected by filtration, washed with ethanol, and dried in vacuo. Yield: 312 mg. Anal. Calcd for $C_{31}H_{40}N_6O_{13.5}Co_2Cl_{2.25}Na_{0.25}$: C, 40.69; H, 4.41; N, 9.18; Na, 0.63. Found: C, 40.40; H, 4.10; N, 9.07; Na, 0.61. IR (cm^{-1}): ν(OH), 3444; ν(C=C), 1608; ν_{as}(COO), 1558; ν_s(COO), 1444; $\nu_3(ClO_4)$, 1084. UV−vis (λ_{max}, cm^{-1} (ϵ, mol^{-1} dm^3 cm^{-1}) in acetonitrile): 22 700 (179); 21 120 (194); 20 200 (191); 17 830 (154), 14 460 (20).

Oxygenation Studies. The equilibrium constant (K) of eq 1 for the oxygenation reaction was determined by spectrophotometric titration in CH_2Cl_2 at −40 °C. The oxygen affinities were estimated by

$$[Fe_2] + O_2 \xrightarrow{K} [Fe_2(O_2)] \quad (1)$$

measuring changes in the relative absorbance of the dioxygen complexes. Measurements were performed with a two-necked Schlenk

vessel with a balloon to keep the inner pressure constant. In the one neck, an optical fiber was placed to monitor the absorbance, and the other neck was sealed with a septum to inject O_2 gas by a syringe. The oxygen partial pressure inside the vessel was estimated from the O_2/N_2 ratio measured by gas chromatographic (GC) analyses. The O_2/N_2 ratio was calibrated using the authentic samples. HITACHI 502 gas chromatography was used with a 2-m column of molecular sieve 5A. The typical experimental procedure was as follows. The complex was dissolved in CH_2Cl_2 under N_2 gas. Then the reaction cell was placed in a constant temperature bath at −40 °C with magnetic stirring. The partial oxygen pressure was varied by injecting the appropriate amount of O_2 gas with a pressure-lock syringe. After an equilibrium was confirmed from the spectral change, the absorbance was measured and the mixed gas in the vessel was analyzed by GC measurements to determine the oxygen partial pressure.

The equilibrium constant (K) was calculated by the following equation: $P(O_2) = CP(O_2)/\Delta A - K^{-1}$, where $P(O_2)$ is the partial pressure of O_2, ΔA is the difference between the absorbances of the solution at $P(O_2)$ and $P(O_2) = 0$ Torr, and C is a constant.[26] Plots of $P(O_2)$ vs $P(O_2)/\Delta A$ for **1** and **2** gave a straight line (Figure S2, supporting information), indicating a 1:1 (complex:O_2) stoichiometry for the oxygenation. The Hill's plots also indicated a 1:1 stoichiometry for the oxygenation reactions.

Physical Measurements. Electronic spectra were measured on a Hitachi U-3400 spectrophotometer, and for low-temperature measurement, an Otuka Denshi optical glass fiber attachment was used. The magnetic susceptibilities were measured with a SQUID susceptometer, QUANTUM DESIGN MPMS Model, which was calibrated with Hg[Co(NCS)$_4$]. Diamagnetic correction was made using Pascal's constants.[27]

Cyclic voltammograms were obtained with a Hokuto Denko HA-301 potentiostat/galvanostat and a Hokuto Denko HB-104 function generator using a three-electrode configuration, including a glassy carbon working electrode, a platinum coil auxiliary electrode, and a saturated calomel electrode as a reference electrode. CH_2Cl_2 was used as a solvent and tetrabutylammonium perchlorate as a supporting electrolyte. The $E_{1/2}$ value of ferrocene/ferrocenium (Fc/Fc^+) was 540 mV with this setup. Constant-potential electrolyses were performed with a Hokuto Denko HA-301 Potentiostat/Galvanostat using a two-compartmental H-type cell separated by a poly(propylene) film (JURAGUARD-2500). The cell was equipped with a platinum gauze working electrode, a platinum plate auxiliary electrode, and a saturated calomel electrode as a reference electrode. Solutions were thoroughly degassed with argon, and all voltammetric measurements were recorded under a positive pressure of argon.

^{1}H NMR spectra were measured by a JEOL GS 400 spectrometer. The 1D spectra were collected over a 160 kHz bandwidth with 16 000 data points and a 8-μs 90° pulse. For a typical spectrum, 1000−4000 transients were accumulated with a 30-ms pulse delay time. The residual ^{1}H spectrum of CD_2Cl_2 was used as a secondary reference. To obtain T_1 values, an inversion recovery sequence was used with τ values varying between 0.1 and 100 ms.

The COSY spectra were obtained after collecting standard 1D reference spectra. The 2D spectrum was collected using 1024 points in t_2 over the bandwidth of 30 kHz with 128 t_1 blocks and 200 scans per block. A 0°-shifted sine bell combined with a Gaussian function was applied in both dimensions and zero-filled to 1024 t_2 × 1024 t_1 data points prior to Fourier transformation and symmetrization.

Raman scattering was excited at 632.8 nm with a He−Ne laser (NEC GLS 5800) and detected with a photodiode array (PAR 1420Q) attached to a double monochromator (SPEX 1404). Raman shifts were calibrated with indene as a standard with an accuracy of ±1 cm^{-1}. All measurements were carried out with a spinning cell (diameter = 2 cm). The cell was spun at 1600 rpm in a cryostat that was cooled to −40 °C by cold N_2 gas. The laser power was 15 mW, and the exposure time was 10 (s) × 70 (repetition), that is 11 min 40 s for measurement of one spectrum.

(26) (a) Rose, N. J.; Drago, R. S. *J. Am. Chem. Soc.* **1959**, *81*, 6138−6141. (b) Collman, J. P.; Brauman, J. I.; Doxsee, K. M.; Halbert, T. R.; Hayes, S. E.; Suslick, K. S. *J. Am. Chem. Soc.* **1978**, *100*, 2761−2766.

(27) Mabbs, F. E.; Marchin, D. J. *Magnetisms and Transition Metal Complexes*; Chapman and Hall: London, 1975; p 5.

Table 1. Crystallographic Data for $[Fe_2(Me_4\text{-tpdp})(C_6H_5COO)(H_2O)](BF_4)_2$ (**1**)

formula	$C_{38}H_{44}N_6O_4Fe_2B_2F_8$
temp, K	296
MW	934.1
cryst system	monoclinic
space group	$P2_1/n$
a, Å	19.257(2)
b,Å	17.166(3)
c, Å	12.558(2)
β,deg	96.55(1)
V,Å^3	4124(1)
$F(000)$	1936
Z	4
D_{calcd}, g/cm^3	1.50
abs coeff, cm^{-1}	8.12
no. of reflns collcd	12882
no. of indpt reflns	6138 ($\geq 6\sigma\|F_o\|$)
no. of refined params	721
largest peak/hole, e Å^{-3}	0.34/−0.16
R^a	0.0458
$R_w{}^b$	0.0581

^{a} $R = \sum[|F_o| - |F_c|/\sum|F_o|]$. ^{b} $R_w = [\sum w(|F_o| - |F_c|)^2/\sum w|F_o|^2]^{1/2}$; $w = 1/\sigma^2(F_o) + g(F_o)^2$; $g = 0.018$.

The Mössbauer spectra were measured using a constant-acceleration spectrometer (Austin Science Associate). The data were stored in a 1024-channel analyzer (type 5200, Inotec Inc.). The spectra were analyzed at the Computer Center of Kyushu University, and the velocity scale was normalized to an iron foil at room temperature. The Mössbauer parameters were obtained from the least-squares fits of the experimental data to Lorentzian line shapes.

Collection and Reduction of X-ray Data. A crystal of **1** suitable for single-crystal X-ray diffraction was grown from methanol−water. An epoxy-covered crystal was mounted on a Rigaku AFC-5R four-circle automated diffractometer equipped with Mo Kα (0.710 73 Å) and a graphite monochrometor. Crystallographic data are summarized in Table 1. Unit cell parameters were determined from the θ values of 25 carefully centered reflections, having $25.0 < 2\theta < 37.0°$. Intensities of three standard reflections were measured during data collection and did not show any systematic decay throughout data monitoring. The data were corrected for absorption by the semiempirical method using Ψ scans and for Lorentz and polarization effects.

Structure Solution and Refinement. The structure of **1** was solved by the conventional heavy-atom techniques. The metal atom was located by Patterson syntheses using the program SHELXS-86.[28] Full-matrix least-squares refinement and difference Fourier methods (SHELX-76[29]) were used to locate all remaining non-hydrogen atoms. The atomic scattering factors were taken from a standard source.[30] Final atomic coordinates and thermal parameters are included as supporting information. All the calculations were carried out on a FACOM M760/20 computer at the Kanazawa University Information Processing Center.

Results

It is well-known that the dioxygen−iron complexes are highly susceptible to irreversible oxidation compared to the corresponding cobalt complexes with the same ligand system. For example, a dinuclear iron(II) complex $[Fe_2(tpdp)(C_6H_5COO)](BPh_4)_2\cdot H_2O$ is very air-sensitive and irreversibly oxidized even at −40 °C in acetonitrile, whereas the corresponding cobalt(II) complex $[Co_2(tpdp)(CH_3COO)]^{2+}$ does not react with O_2 at room temperature but reversibly binds O_2 in acetonitrile below 0 °C to form a μ-peroxo complex. In order to suppress such irreversible oxidation of the iron(II) ion, we have developed new dinucleating ligands (Me_4-tpdp and Me_2-tpdp) with steri-

(28) Sheldrick, G. M. *SHELXS-86*. A Program for Crystal Structure Determination; University of Göttingen: FRG, 1986.

(29) Sheldrick, G. M. *SHELX-76*. A Program for Crystal Structure Determination; Cambridge University: Cambridge, U.K., 1976.

(30) *International Tables for X-ray Crystallography*; Kynoch Press: Birmingham, England, 1974; Vol. IV.

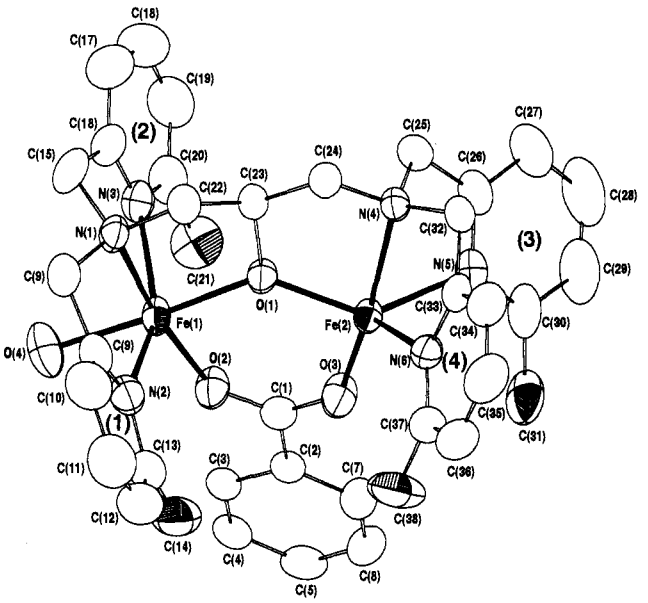

Figure 1. ORTEP view of complex cation $[Fe_2(Me_4\text{-tpdp})(C_6H_5COO)(H_2O)](BF_4)_2$ (**1**) with the atom numbering scheme. The non-hydrogen atoms are represented by 50% probability thermal ellipsoids. The hydrogen atoms are omitted for clarity. (1)–(4) denote 6-methylpyridyl planes.

Table 2. Selected Bond Lengths and Bond Angles of $[Fe_2(Me_4\text{-tpdp})(C_6H_5COO)(H_2O)](BF_4)_2$ (**1**)

Bond Lengths (Å)			
Fe(1)···Fe(2)	3.684 (1)	Fe(1)–N(3)	2.337 (3)
Fe(1)–O(1)	2.060 (2)	Fe(2)–O(1)	1.984 (2)
Fe(1)–O(2)	2.066 (2)	Fe(2)–O(3)	1.995 (2)
Fe(1)–O(4)	2.142 (3)	Fe(2)–N(4)	2.195 (2)
Fe(1)–N(1)	2.200 (3)	Fe(2)–N(5)	2.202 (3)
Fe(1)–N(2)	2.287 (3)	Fe(2)–N(6)	2.175 (3)
Bond Angles (deg)			
Fe(1)–O(1)–Fe(2)	131.2(1)	O(3)–Fe(2)–N(5)	96.5(1)
O(2)–Fe(1)–N(2)	105.3(1)	O(3)–Fe(2)–N(6)	120.0(1)
O(2)–Fe(1)–N(3)	103.0(1)	N(4)–Fe(2)–N(5)	74.9(1)
N(1)–Fe(1)–N(2)	76.7(1)	N(4)–Fe(2)–N(6)	77.1(1)
N(1)–Fe(1)–N(3)	76.6(1)		

cally hindered nitrogen bases (6-methylpyridyl groups). The 6-methyl group in the pyridyl group would be expected to weaken the electron donor ability of the pyridyl nitrogen because of its unfavorable steric requirement upon coordination and to stabilize the iron(II) oxidation state (vide infra).

X-ray Structure Description of 1. The molecular structure of the dinuclear cation of **1** is shown in Figure 1. The selected bond distances and angles are given in Table 2. The dinuclear complex cation consists of two distinct iron centers, one five- and one six-coordinate, which are doubly bridged by the alkoxide oxygen of Me_4-tpdp and the benzoate oxygens. The five-coordinate iron center has a distorted trigonal bipyramidal structure with three nitrogens of Me_4-tpdp and two oxygens of Me_4-tpdp and benzoate, where the tertiary amine nitrogen and the bridging benzoate oxygen are in the apical position. The six-coordinate center contains an additional coordinated water molecule to form a distorted octahedral structure with an N_3O_3 donor set where three nitrogens of Me_4-tpdp are in a meridional form.

The Fe-N(pyridyl) and Fe–O bond distances in the six-coordinate Fe(1) center are substantially longer than those in the five-coordinate Fe(2) center except for the Fe–N(tertiary amine) bonds. Similar observation was made for $[Fe_2(O_2CH)_4(BIPhMe)_2]$, as reported by Lippard et al.[15b] The average Fe–N(pyridyl) bond distances for Fe(1) and Fe(2) are 2.31 and 2.19 Å, respectively. The Fe–N(aromatic) bond distances found for six-coordinate complexes are in the range 2.14–2.22 Å ($[Fe_2(O_2CH)_4(BIPhMe)_2]$,[15b] 2.14 Å; $[Fe_2(OCCH_3)_2(TPA)](BPh_4)_2$,[19] 2.18 Å; $[Fe_2(bpmp)(O_2CC_2H_5)_2]BPh_4$,[16c] 2.20 Å; $[Fe(TLA)BF]ClO_4$,[31] 2.22 Å), and those for five-coordinate complexes are in the range 2.07–2.17 Å ($[Fe_2(N\text{-Et-HPTB})(O_2CC_6H_5)](BF_4)_2$,[22] 2.07 Å; $[Fe_2(O_2CH)_4(BIPhMe)_2]$,[15b] 2.12 Å; $[Fe(HB(3,5\text{-}iPr_2pz)_3]_2(OH)(O_2CC_6H_5)$,[17] 2.15 Å; $[Fe(HB(3,5\text{-}iPr_2pz)_3]_2(OH)_2$,[17] 2.17 Å). Thus, introduction of a methyl group into the 6-position of the pyridyl group causes a significant elongation of the Fe–N(pyridyl) bonds. Similar observations have been made for the complexes with a 6-methylpyridyl group.[32]

The elongation of the Fe–N(pyridyl) bonds seems to be partly due to unfavorable steric interaction between the hydrogen atoms of the 6-methyl group and oxygen atoms of the bridging benzoate. In the six-coordinate iron center, the 6-methyl groups are almost directed to the O(2) atom; the dihedral angles between the 6-methylpyridyl planes (1) and (2), which are shown in Figure 1, and the planes defined by Fe(1), O(2), and pyridyl nitrogens (N(2) and N(3)) are 13 and 16°, respectively, and the deviations of the methyl groups from the planes defined by Fe(1), O(2), and pyridyl nitrogens (N(2) and N(3)) are 0.12 and 0.08 Å, respectively. Such an orientation of the methyl groups may prevent a close approach of the pyridyl nitrogen to avoid unfavorable steric interaction between the methyl groups and the O(2) atom. The separations of the O(2)··C(14) and O(2)··C(21) are 3.157(5) and 3.178(6) Å, respectively. On the other hand, in the five-coordinate iron center which has shorter Fe–N(pyridyl) bond distances, one methyl group (C(31)) is not directed to the O(3) atom so as to avoid unfavorable short contact; the dihedral angle between the 6-methylpyridyl plane (3) and the plane defined by Fe(2), O(3), and N(5) atoms is 44°, and the deviation of the methyl group from the plane (Fe(2), O(3), and N(5)) is 1.73 Å. This leads to the O(3)··C(31) separation of 3.234(6) Å. The other methyl group (C(38)) is almost directed to the O(3) atom (dihedral angle = 16° and the deviation of the methyl group from the corresponding plane = 0.617 Å), resulting in a substantial expansion of the O(3)–Fe(2)–N(6) angle (120.0(1)°) relative to those of the other corresponding angles (96.5(1)°–105.3(1)°), and the O(3)··C(38) separation is 3.438(6) Å.

Comparison of the structure of **1** with that of a closely related dinuclear iron(II) complex, $[Fe_2(NEt\text{-}HPTB)(OBz)](BF_4)_2$ (**6**) reported by Que et al.,[22] reveals some interesting points, where NEt-HPTB has 2-benzimidazolylmethyl groups as side arms. Unlike **1**, each iron center in **6** has a five-coordinate structure. The Fe–N(benzimdiazolyl) bond distancs in **6** are in the range 2.06–2.08 Å, which are considerably shorter than the Fe(2)–N(pyridyl) bond distances in the five-coordinate center of **1**, suggesting that the benzimidazolyl group is a stronger base than the 6-methylpyridyl group. Complex **6** has substantially longer Fe–N(tertiary amine) bonds (2.318(8) and 2.28(1) Å) compared to the Fe–N(benzimidazolyl) bonds. The Fe–N(tertiary amine) bonds have been shown to be longer than the Fe–N(aromatic) bonds in a variety of iron complexes of various tripodal ligands such as tris(2-pyridylmethyl)amine.[16c,19,33] In contrast, this is

(31) Chiou, Y.-M.; Que, L., Jr. *J. Am. Chem. Soc.* **1992**, *114*, 7567–7568.

(32) (a) Goodson, P. A.; Hodgson, D. J. *Inorg. Chem.* **1989**, *28*, 3606–3608. (b) Goodson, P. A.; Oki, A. R.; Glerup, J.; Hodgson, D. J. *J. Am. Chem. Soc.* **1990**, *112*, 6248–6254.

(33) (a) Chen, Q.; Lynch, J. B.; Gomez-Romero, P.; Ben-Hussein, A.; Jameson, G. B.; O'Connor, C. J.; Que, L., Jr. *Inorg. Chem.* **1988**, *27*, 2673–2681. (b) Norman, R. E.; Yan, S.; Que, L., Jr.; Backes, G.; Ling, J.; Sanders-Loehr, J.; Zhang, J. H.; O'Connor, C. J. *J. Am. Chem. Soc.* **1990**, *112*, 1554–1562 and references therein.

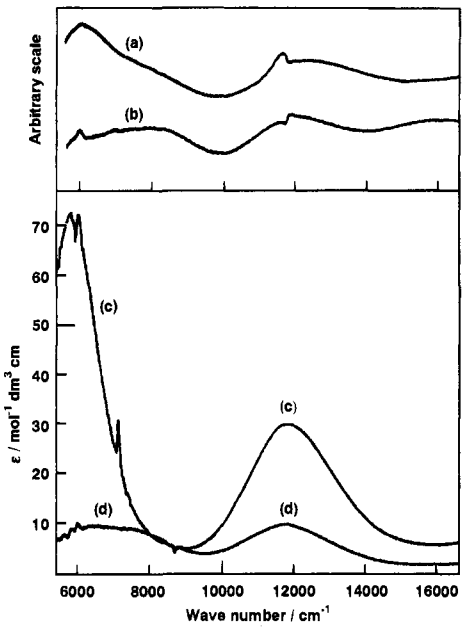

Figure 2. Reflectance spectra of $[Fe_2(Me_4\text{-tpdp})(C_6H_5COO)(H_2O)](BF_4)_2$ (**1**) (a) and $[Fe_2(Me_4\text{-tpdp})(CF_3COO)(H_2O)_2](BF_4)_2$ (**2**) (b), and absorption spectra of **1** in CH_2Cl_2 (c) and in DMSO (d).

not the case for **1**. Similar observations were made for the complexes having 6-methylpyridyl groups ($[Fe(TLA)BF]ClO_4$,[31] $Fe-N_{av}$(pyridyl) = 2.22 Å and Fe−N(tertiary amine) = 2.171(5) Å; $[Fe_4(Me_4\text{-tpdp})_2(F)_2(OH)_2(H_2O)_2](BF_4)_4$,[34] $Fe-N_{av}$(pyridyl) = 2.28 Å and Fe−N(tertiary amine) = 2.18(1) Å). These facts suggest that weakly coordinated side arms in the tripodal ligand tend to strengthen the Fe−N(tertiary amine) bonds and make them shorter. The Fe(2)−N(tertiary amine) bond distance in the five-coordinate iron center is comparable to the Fe(2)−N(pyridyl) bond distances, whereas that in the six-coordinate iron center is significantly shorter than the Fe(1)−N(pyridyl) bond distances. This implies that the 6-methylpyridyl nitrogens in the six-coordinate iron center appear to function as weaker donors than those in the five coordinate iron center, in line with longer Fe(2)−N(pyridyl) bond distances.

Electronic Spectra. The d−d transitions of high-spin iron(II) complexes provide valuable information on the stereochemistry around the iron(II) center; for six-coordinate complexes, the electronic transitions from $^5T_{2g}$ to ^5E_g (in octahedral symmetry) have been shown to split into two bands with a splitting of 1000−2000 cm^{-1} and appear at about 10 000 cm^{-1}, while for five-coordinate complexes, the splitting is much larger than that of six-coordinate complexes and their electronic spectra display two d−d bands near 10 000 cm^{-1} and near 5000 cm^{-1}.[35] The reflectance spectrum of **1**, which contains both five- and six-coordinate iron(II) centers, shows three d−d bands at 12 400 cm^{-1}, ~8000 cm^{-1} (shoulder), and ~6000 cm^{-1} (Figure 2 and Table 3). The bands at 12 400 and ~6000 cm^{-1} can be assigned to the d−d transitions of a five-coordinate iron(II) center and the bands at 12 400 and ~8000 cm^{-1} (shoulder) to those of a six-coordinate iron(II) center. The splitting of the latter two bands is substantially larger than those of the six-coordinate iron(II) complexes so far reported. This seems to reflect a significant distortion from octahedral symmetry in the six-coordinate iron center. The reflectance spectrum of **2**, however, showed only two bands at 12 000 and ~8000 cm^{-1} (broad), indicating that the complex contains six-coordinate iron centers.

Table 3. Electronic Spectral Data of $[Fe_2(Me_4\text{-tpdp})(C_6H_5COO)(H_2O)](BF_4)_2$ (**1**) and $[Fe_2(Me_4\text{-tpdp})(CF_3COO)(H_2O)_2](BF_4)_2\cdot H_2O$ (**2**)

complexes	band maxima $\bar{\nu}$, cm^{-1} (ϵ, mol^{-1} dm^3 cm^{-1})		
1			
reflectance	~12 400	~8000[a]	~6000
in CH_2Cl_2	11 850 (30)		~5800 (~70)
in CH_2Cl_2/DMSO (8:2 v/v)	11 720 (17)		6000−5000
in DMSO	11 790 (10)	8000−6300 (~9)	
2			
reflectance	~12 000	~8000[b]	
in CH_2Cl_2	11 980 (18)		~6100 (~35)
in DMSO	11 740 (7)	7770[b] (9)	
deoxy-Hr[c]	11 600 (10−15)	8770 (~6)[a]	5000 (6−10)
deoxy-N_3-Hr[c]	10 600 (~22)	8500 (~7)[a]	

[a] Shoulder. [b] Broad band. [c] Reference 34.

It should be noted that the absorption spectrum of **1** in CH_2Cl_2 displays only two absorption bands at 11 850 cm^{-1} (ϵ = 30 mol^{-1} dm^3 cm^{-1}) and ~5800 cm^{-1} (ϵ = ~70 mol^{-1} dm^3 cm^{-1}) (Figure 2). The spectral change in CH_2Cl_2 clearly indicates that the dissociation of a coordinated water molecule occurs and each iron center has a five-coordinate structure. The same observation was made for **2** in CH_2Cl_2. The absorption spectra of these complexes showed a significant solvent effect. The absorption spectrum of **1** in DMSO shows bands at 11 790 and 8000−6300 cm^{-1}, suggesting the coordination of DMSO and substantial formation of the six-coordinate species. The spectrum in CH_2Cl_2 containing 20% DMSO is an intermediate spectrum relative to those in CH_2Cl_2 and DMSO, suggesting that there is an equilibrium between five- and six-coordinate species. A similar equilibrium has been suggested for the reaction of $[Fe_2(N\text{-Et-HPTB})(C_6H_5COO)]^{2+}$ with DMSO by NMR study.[22b]

Magnetism. The temperature dependence of the magnetic susceptibility of a powdered sample of **1** was measured in the range 300−10 K (Figure 3). The effective magnetic moment (Fe_2) decreases from 6.69 μ_B at 300 K to 1.71 μ_B at 10 K, indicating the presence of an antiferromagnetic exchange interaction between two high-spin iron(II) ions. The magnetism was analyzed by the isotropic exchange interaction model $H = -2JS_1\cdot S_2$ ($S_1 = S_2 = 2$). The magnetic susceptibility data were fitted to the following equation:

$$\chi_M = \frac{2N\beta^2g^2}{kT}\frac{30 + 14x^8 + 5x^{14} + x^{18}}{9 + 7x^8 + 5x^{14} + 3x^{18} + x^{20}}(1 - \mathrm{PIP}) + \frac{3.00}{T}\mathrm{PIP}$$

where $x = \exp(-J/kT)$ and the symbols have their usual meanings and PIP is a paramagnetic impurity ($S = {}^5/_2$). The least-squares fitting shown as a solid line in Figure 3 gave g = 2.11, J = −8.6 cm^{-1}, and PIP = 0.02. A deviation of the theoretical curve from the experimental data in the low-temperature region may be due to spin−orbit coupling which was neglected in this study. The magnitude of the antiferromagnetic exchange constant for **1** is comparable to those reported for **6** (J = −10.5 cm^{-1}),[22b] $[Fe_2(OH)(CH_3COO)_2(Me_3TACN)_2]ClO_4$ (J = −13 cm^{-1}),[14b] and deoxy-Hr (−13 cm^{-1} and −25 ± 13 cm^{-1}).[35,36]

Mössbauer Spectra. The Mössbauer spectrum of **1** measured at room temperature is given in Figure 4. The asymmetric nature of the two iron centers in **1** is apparent from the presence

(34) The complex is a tetranuclear high-spin iron(II,III,II,III) mixed-valence complex with a rectangular array. Hayashi, Y.; Sugimoto, H.; Suzuki, M.; Maeda, Y.; Uehara, A. Manuscript in preparation.

(35) Reem, R. C.; Solomon, E. I. *J. Am. Chem. Soc.* **1987**, *109*, 1216−1226.

(36) Maroney, M. J.; Kurtz, D. M., Jr.; Nocek, J. M.; Pearce, L. L.; Que, L., Jr. *J. Am. Chem. Soc.* **1986**, *108*, 6871−6879.

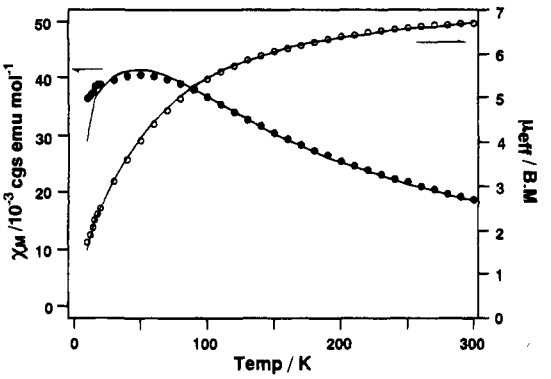

Figure 3. Temperature dependence of magnetic susceptibilities (χ_M) for $[Fe_2(Me_4\text{-tpdp})(C_6H_5COO)(H_2O)](BF_4)_2$ (**1**). The solid line is a theoretical curve with $J = -8.6$ cm^{-1}, $g = 2.11$, and PIP = 0.02 paramagnetic impurity ($S = {}^5/_2$).

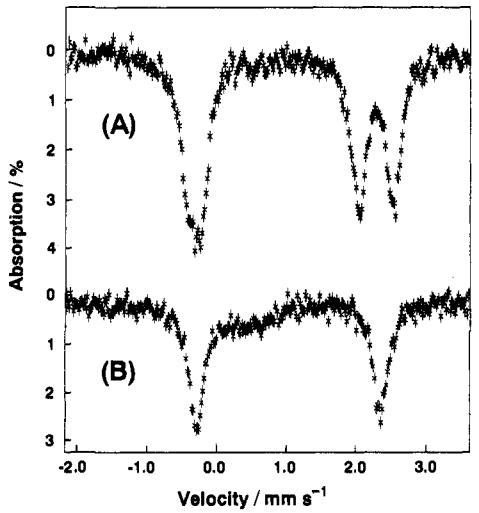

Figure 4. Mössbauer spectra of $[Fe_2(Me_4\text{-tpdp})(C_6H_5COO)(H_2O)](BF_4)_2$ (**1**) (A) and $[Fe_2(Me_4\text{-tpdp})(CF_3COO)(H_2O)_2](BF_4)_2$ (**2**) (B) at 300 K.

of the two pairs of quadrupole doublets, which are consistent with two distinct iron centers. There are two possible pairs of quadrupole doublets for two distinct iron centers; one possible pair of quadrupole doublets is $\delta_1 = 0.92$ mm s^{-1} and $\Delta E_{Q1} = 2.30$ mm s^{-1} and $\delta_2 = 1.08$ mm s^{-1} and $\Delta E_{Q2} = 2.98$ mm s^{-1}, and the other is $\delta_1 = 0.83$ mm s^{-1} and $\Delta E_{Q1} = 2.48$ mm s^{-1} and $\delta_2 = 1.17$ mm s^{-1} and $\Delta E_{Q2} = 2.80$ mm s^{-1}. In either case, the parameters are in the range of those for the high-spin iron(II) complexes. The spectrum is in contrast to that of deoxy-Hr, which shows only one quadrupole doublet, although it also has two distinct iron centers, one five-coordinate and one six-coordinate iron center, as does **1**. Thus unsymmetry of electron density distributions around the two iron centers in **1** is larger than that in deoxy-Hr and large enough to afford two distinct quadrupole doublets.

In contrast, the Mössbauer spectrum of **2** shows a single quadrupole doublet with $\delta = 1.05$ mm s^{-1} and $\Delta E_Q = 2.69$ mm s^{-1}, consistent with the observation that the complex contains two six-coordinate iron centers in the solid state.

^{1}H NMR Spectra. Figure 5 shows the ^{1}H NMR spectrum of **1** in CD_2Cl_2 which exhibits well-resolved paramagnetically shifted resonances that span over 200 ppm. The assignment of the resonances was made on the basis of their relative intensities, T_1 values, and the number of the resonances observed. Complex **1** has five types of protons: methylene protons (H_a and H_e), methine proton (H_t), methyl protons (Me and Me′), pyridyl protons (Pm_1, Pp, Pm_2, Pm_1′, Pp′, and Pm_2′), and benzoate

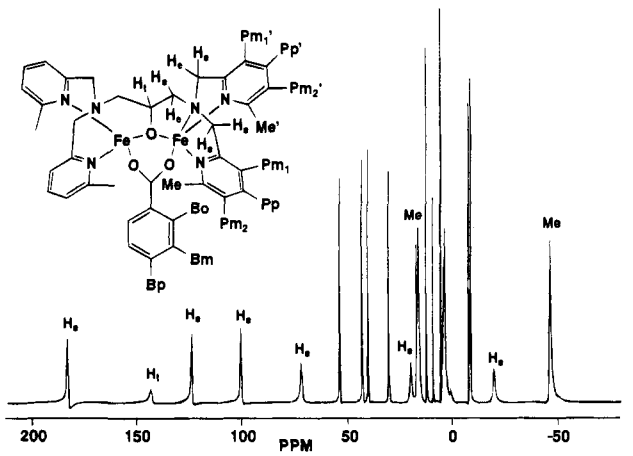

Figure 5. ^{1}H NMR spectrum of $[Fe_2(Me_4\text{-tpdp})(C_6H_5COO)(H_2O)](BF_4)_2$ (**1**) in CD_2Cl_2 at 300 K.

protons (Bo, Bm, and Bp) as shown in the inset of Figure 5. The methylene proton has an axial (Ha) or equatorial (H_e) orientation with respect to the chelate ring. The equatorial protons have longer Fe−H distances than the corresponding axial protons, leading to longer relaxation time. The sharper resonances at 182.9, 124.1, and 100.6 ppm with T_1 values of ~3 ms can be tentatively assigned to the methylene protons in the equatorial positions, and the broader resonances at 72.0, 20.0, and −19.5 ppm with T_1 values of <1 ms are assigned to the protons at the axial positions. The methine proton (H_t) appears as a broad signal at 143.5 ppm, which can be identified from its intensity. The methyl protons are assigned to the resonances at 16.4 and −46.3 ppm with T_1 values of ~3 ms. The remaining peaks were assigned by two-dimensional COSY. The observation of three methylene proton signals and two methyl proton signals indicates that the complex cation of **1** has 2-fold symmetry in CH_2Cl_2. This is in accord with the electronic spectral result that the complex has two five-coordinate iron centers. The NMR spectrum of **2** is similar to that of **1** except for the absence of the benzoate protons.

Que et al. have demonstrated that two-dimensional COSY study is useful for the identification of the pyridyl protons in the dinuclear iron(II) complex $[Fe_2(bpmp)(C_6H_5COO)_2]^+$.[37] Resonances due to the pyridyl protons in **1** are clearly identified by the appearance of the cross peaks due to pyridyl proton connectivities (Figure 6). The presence of only two types of cross peaks also supports the belief that the complex has 2-fold symmetry. The cross peaks in the benzoate protons (B_m and B_p protons) are also observed. However, it was difficult to observe cross peaks between the benzoate B_o and B_m protons and the axial and equatorial methylene protons which have shorter T_1 values.

Electrochemistry. Cyclic voltammograms (CV) of **1** and **2** in CH_2Cl_2 showed two quasi-reversible waves, which correspond to Fe_2(II,III)/Fe_2(II,II) and Fe_2(III,III)/Fe_2(II,III) redox couples. The $E_{1/2}$ values of Fe_2(II,III)/Fe_2(II,II) and Fe_2(III,III)/Fe_2(II,III) couples in CH_2Cl_2 are 605 and 995 mV vs SCE for **1** and 750 and 1260 mV vs SCE for **2**, respectively. Thus the $E_{1/2}$ values of these complexes are well correlated with the electron donor ability of the bridging carboxylates; benzoate is more basic than trifluoroacetate.

Oxygenation Reaction. Complex **1** does not form an oxy complex and undergoes an irreversible oxidation at ambient temperature. Complex **2** binds O_2 in CH_2Cl_2 even at ambient temperature with an instantaneous color change from pale yellow to deep blue. However, the oxy-**2**, which is thermally more

(37) Ming, L.-J.; Jang, H. G.; Que, L., Jr. *Inorg. Chem.* **1992**, *31*, 359–364.

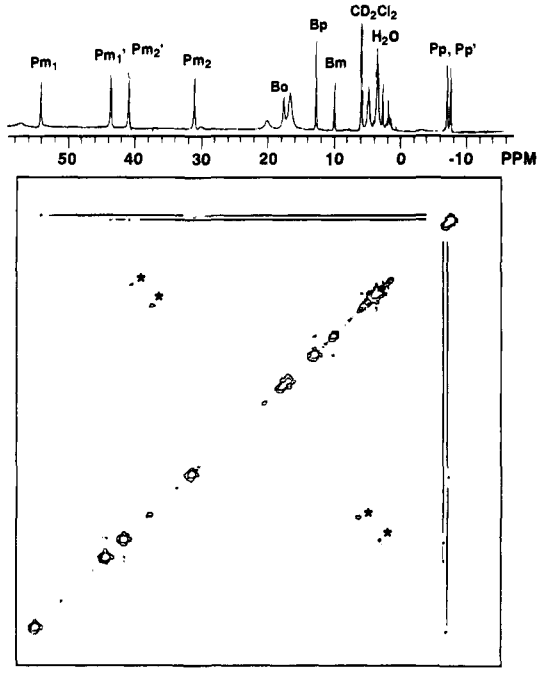

Figure 6. COSY spectrum of $[Fe_2(Me_4\text{-tpdp})(C_6H_5COO)(H_2O)](BF_4)_2$ (**1**) in CD_2Cl_2 at 300 K. The asterisked peaks are folding peaks.

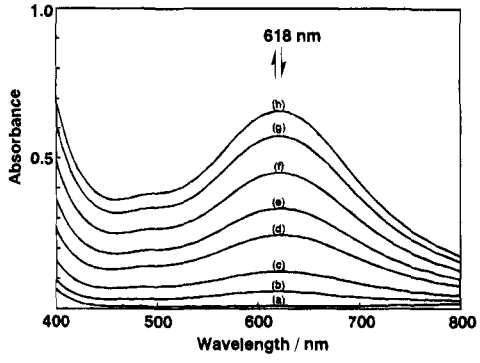

Figure 7. Absorption spectral changes of $[Fe_2(Me_4\text{-tpdp})(CF_3COO)(H_2O)_2](BF_4)_2$ (**2**) in CH_2Cl_2 at −40 °C at various partial pressures of O_2. Spectra a−h are at the partial pressures of O_2: (a) 0, (b) 2, (c) 6, (d) 16, (e) 26, (f) 49, (g) 79, and (h) 135 Torr, respectively.

stable than oxy-**1**, is not stable at ambient temperature and is irreversibly oxidized within several minutes to give a brown species. Good reversible oxygenation was observed for **1** and **2** below −35 °C; bubbling of Ar gas into the deep blue solution restored the original pale yellow color. Figure 7 shows the spectral change of **2** in CH_2Cl_2 at various oxygen pressures ($P(O_2)$) at −40 °C. Oxy-**1** has an absorption maximum at 616 nm (ϵ = ~2000 $dm^3\ mol^{-1}\ cm^{-1}$). The absorption spectrum of oxy-**2** (λ_{max} = 618 nm (ϵ = ~1000 $dm^3\ mol^{-1}\ cm^{-1}$)) in CH_2Cl_2 resembles that of oxy-**1**.

Complex **3** also reacts rapidly with O_2 to give an oxy complex in acetone and acetonitrile at −60 °C with a color change from yellow to deep blue corresponding to the appearance of a strong absorption band at 603 nm (ϵ = ~1400 $dm^3\ mol^{-1}\ cm^{-1}$). In CH_2Cl_2, oxygenation proceeded very slowly. In contrast to **1** and **2**, deoxygenation was not effected by bubbling of Ar gas through acetonitrile or acetone solution, and oxy-**3** gradually decomposed within a few hours even at −60 °C. Reaction of **4** with O_2 in acetonitrile showed an instantaneous irreversible oxidation even at −40 °C. Que et al. reported that oxy-**4** cannot be formed in CH_2Cl_2 even at −80 °C, although the presence of DMSO greatly stabilizes oxy-**4**.[22b] Thus the thermal stabilities of the oxygenated complexes toward irreversible oxidation are

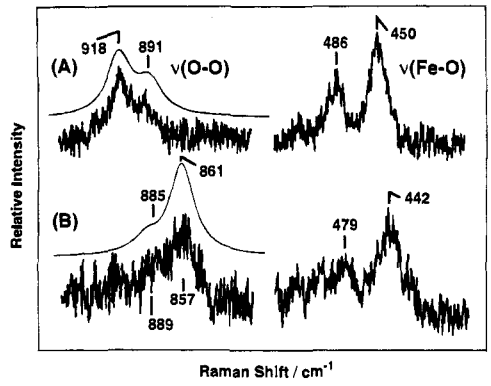

Figure 8. Resonance Raman spectra of $[Fe_2(Me_4\text{-tpdp})(C_6H_5COO)(H_2O)](BF_4)_2$ (**1**) in CH_2Cl_2 at −40 °C: (A) $^{16}O_2$, (B) $^{18}O_2$. The solid lines are the simulated spectra (see text).

highly dependent on the dinucleating ligands: Me_4-tpdp > Me_2-tpdp > tpdp. This order correlates well with the relative degree of steric bulkiness and the electron donor ability of the dinucleating ligands.

As mentioned before, although **1** is irreversibly oxidized in dichloromethane at ambient temperature, in CH_2Cl_2 containing 20% DMSO, it reacts with O_2 to form an oxy complex and shows reversible oxygenation−deoxygenation to some extent even at ambient temperature. Thus, the presence of DMSO greatly stabilizes the oxy complex. This is probably due to a polar solvent effect as noted by Que et al.[22b] However, the reaction rate of the oxygenation of **1** and **2** was significantly decreased in CH_2Cl_2 containing 20% DMSO as the temperature decreased. The oxygenation of the complexes in this mixed solvent took several hours at −60 °C, while they were oxygenated within several minutes in dichloromethane. The reaction of **1** and **2** with O_2 in DMSO showed only a faint green color at ambient temperature, suggesting a slight oxygenation. The complexes were gradually oxidized to give a brown color.

It is interesting to investigate the factors which affect the oxygen affinity of diiron(II) complexes of various dinucleating ligands. Because complexes **1** and **2** show reversible oxygenation in CH_2Cl_2, we measured the oxygen affinity. $P(O_2)_{1/2}$ values for **1** and **2** are estimated to be ca. 6 and ca. 41 Torr, respectively, in CH_2Cl_2 at −40 °C. A thermodynamic study of the oxygenation of these complexes along with other diiron(II) complexes of various dinucleating ligands is under investigation.[38] Very recently, a mechanistic study of the oxygenation of complexes **1**, **4**, and **6** in propionitrile has been reported.[39]

Raman Spectra. Figure 8 shows the resonance Raman spectra of oxy-**1** in CH_2Cl_2 at −40 °C obtained with a spinning cell. As shown in Figure 8A, the $^{16}O_2$ derivative of oxy-**1** gives two RR bands at 486 and 450 cm^{-1} in the Fe−O stretching region and a doublet band with peaks at 918 and 891 cm^{-1} in the O−O stretching region. With the use of $^{18}O_2$, the 486 and 450 cm^{-1} bands shift to 479 and 442 cm^{-1}, respectively (Figure 8B) and the doublet band around 900 cm^{-1} of the $^{16}O_2$ derivative downshifts to a doublet at 889 and 857 cm^{-1}, although their relative intensities are reversed between the $^{16}O_2$ and $^{18}O_2$ derivatives. Therefore, these bands are associated with the vibrations involving oxygen. The observed $^{18}O_2$ isotopic frequency shifts (−7 to −8 cm^{-1}) for the low-frequency bands are considerably smaller than those expected for the isolated Fe−O_2 (or Fe−O) stretching mode which is calculated to be −17 and −16 cm^{-1} in the case of Fe−O_2 stretching (−21 and

(38) Sugimoto, H.; Hayashi, Y.; Suzuki, M.; Uehara, A. Manuscript in preparation.

(39) Feig, A. L.; Lippard, S. J. *J. Am. Chem. Soc.* **1994**, *116*, 8410−8411.

-20 cm^{-1} in the case of Fe−O stretching) for the 486 and 450 cm^{-1} modes, respectively. This suggests that the Fe−O_2 stretching modes are coupled with other vibrations. The resonance Raman spectra of oxy-**2** and oxy-**3** are quite similar to that of oxy-**1**. The O−O stretching and the Fe−O stretching Raman bands disappeared when we stopped spinning the cell. This shows that the oxy species are photolabile and that our technique is suitable for RR measurements of such photolabile species. The presence of two bands in the O−O stretching region will be discussed in detail later.

Discussion

As mentioned before, all the complexes showed two Fe−O_2 stretching bands. The presence of those bands may imply the presence of two isomers. However, the oxygen affinity measurement gave no evidence of the presence of two oxy species. In addition, the relative intensities of those two bands for **1** exhibited little change in response to various environmental changes such as rising temperature or addition of methanol to the solvent. The intensity ratios of the two Fe−O_2 bands for **2** and **3** are similar to that of **1**. These observations suggest that the two pairs of oxygen-isotope sensitive Raman bands arise from a single species.

The two Fe−O_2 stretching bands can be assigned to the symmetric and antisymmetric combinations of the Fe−O stretching of the Fe−O−O−Fe structure (vide infra). However, interpretation of the doublet around 900 cm^{-1}, which is assigned to the O−O stretching mode (ν(O−O)), is not straightforward. One may argue that the 891-cm^{-1} band in spectrum A corresponds to the 889-cm^{-1} band in spectrum B and thus shows no isotopic shift. If this were true, the 918-cm^{-1} band would be shifted to 857 cm^{-1} with $^{18}O_2$, but a downshift as large as 61 cm^{-1} is quite unreasonable for any mode because it exceeds the frequency shift (-53 cm^{-1}) expected for the isolated O−O oscillator at 918 cm^{-1}. Because the presence of a single oxy-**1** species is likely, another possibility for the observation of two ν(O−O) frequencies may indicate the appearance of a hot band of anharmonic oscillator. If so, the 918- and 891-cm^{-1} bands would be ascribed to $v = 0 \rightarrow 1$ and $v = 1 \rightarrow 2$ transitions, respectively. However, the population at the $v = 1$ level for the 918-cm^{-1} mode is less than 0.003 of that at the $v = 0$ level at -40 °C, and therefore, the intensity of the 891-cm^{-1} band cannot be explained in terms of the hot band. Some satisfactory interpretation of the origin for the presence of two sets of oxygen-isotope sensitive bands and the large magnitude of the isotopic shift of ν(O−O) is quite important in this study; therefore we discuss it in detail below.

The remaining possibility is to assign it to a Fermi doublet as Brennan et al.[20f] suggested. In order to examine the validity of this, we carried out simulation calculations of the doublet bands under the assumption of Fermi resonance. If it is supposed that ν_O^0 and ν_i^0 are the intrinsic frequencies of the O−O stretching and an overtone of some interacting vibration, respectively and that the magnitude of their interactions is W_{Oi}, the first-order perturbation theory predicts the resultant frequencies, $\nu^{(\pm)}$, by eq 2:[40]

$$\nu^{(\pm)} = \nu_{Oi} \pm \gamma/2 \tag{2}$$

where ν_{Oi} and γ are defined by eqs 3−5:

$$\nu_{Oi} = (\nu_O^0 + \nu_i^0)/2 \tag{3}$$

$$\gamma = (4W_{Oi}^2 + \delta^2)^{1/2} \tag{4}$$

$$\delta = \nu_O^0 - \nu_i^0 \tag{5}$$

$\nu^{(\pm)}$ corresponds to the observed frequencies. The vibrational wave functions (Ψ_O and Ψ_i) of the resultant mixed modes are represented by the unperturbed wave functions (Ψ_O^0 and Ψ_i^0) as

$$\Psi_O = a\Psi_O^0 - b\Psi_i^0 \tag{6a}$$

$$\Psi_i = b\Psi_O^0 + a\Psi_i^0 \tag{6b}$$

where

$$a = [(\gamma + \delta)/2\gamma]^{1/2} \quad \text{and} \quad b = [(\gamma - \delta)/2\gamma]^{1/2} \tag{7}$$

Under the ordinary assumption that the intrinsic intensity of the overtone is zero, the intensity ratio, R, of the two resultant bands can be represented by

$$R = (a/b)^2 = (\gamma + \delta)/(\gamma - \delta) \tag{8}$$

We fitted the observed doublet for the $^{16}O_2$ derivative with two Lorentzian functions (solid line in Figure 8A) and obtained the value of $R = 1.8$. Using eqs 2−5 and 8 and the values of $\nu^{(+)} = 918$ cm^{-1}, $\nu^{(-)} = 891$ cm^{-1}, and $R = 1.8$ observed for $^{16}O_2$ derivative, we can calculate the parameters ν_O^0, ν_i^0, and W_{Oi} to be 908, 901, and 12 cm^{-1}, respectively. It is likely that W_{Oi} is common between the $^{16}O_2$ and $^{18}O_2$ derivatives. Then, by using the values of $\nu^{(+)} = 889$ cm^{-1} and $\nu^{(-)} = 857$ cm^{-1} observed for the $^{18}O_2$ derivative and W_{Oi} (12 cm^{-1}), the ν_O^0, ν_i^0, and R values are calculated to be 861 cm^{-1}, 885 cm^{-1}, and 5.8, respectively. The simulated doublet composed of two Lorentzian bands with an intensity ratio of 5.8 is shown by the solid line near the spectrum B in Figure 8. This simulated spectrum is in good agreement with the observed one. This calculation revealed that the intrinsic ν(O−O) frequencies (ν_O^0) for the $^{16}O_2$ and $^{18}O_2$ derivatives are 908 and 861 cm^{-1}, respectively, and therefore its isotopic shift is -47 cm^{-1}, in reasonable agreement with the expected value. Furthermore, the intrinsic overtone frequencies (ν_i^0) are 901 and 885 cm^{-1} for the $^{16}O_2$ and $^{18}O_2$ derivatives, respectively, which are reasonable for the observed fundamentals at 450 and 442 cm^{-1} for the $^{16}O_2$ and $^{18}O_2$ derivatives, respectively. The shoulder band at 889 cm^{-1} is too weak to determine its peak position accurately, but an error of ± 2 cm^{-1} in $\nu^{(+)}$ causes uncertainties of only ± 2 cm^{-1} in ν_O^0 and ν_i^0 and of ± 1.2 in R. These uncertainties do not give rise to any serious problem in the argument described above. In this way, the quantitative treatment under the assumption of Fermi resonance has satisfactorily explained the observed spectral features and the apparent large magnitude of the isotopic frequency shift for the bands observed in the ν(O−O) region within a regime of a single species.

The observed two Fe−O_2 stretching bands are thus assigned to the symmetric and antisymmetric combinations of the Fe−O stretching of Fe−O−O−Fe structure. If the Fe−O−O−Fe part has C_{2h} symmetry, the antisymmetric combination should not be Raman active. Hence, the observation of two Fe−O_2 stretching bands indicates that the Fe−O−O−Fe part should not have a center of symmetry and this feature might be characteristic of the asymmetric structure of oxy-**1**.

Only a few iron(II) complexes which bind O_2 in μ-peroxo form have been reported. Iron(II) complexes are highly susceptible to irreversible oxidation by O_2. It is interesting to investigate the factors which affect the thermal stability (or reversibility) of μ-peroxo diiron complexes. Some factors have been suggested which contribute to the thermal stability of μ-peroxo diiron complexes: (1) the electron donor ability of

(40) Herzberg, G. *Molecular Spectra and Structure*; Van Nostrand: New York, 1945; Vol. 2, p 215.

ligands, (2) a hydrophobic pocket surrounding the O_2-binding site, and (3) solvent polarity.

Introduction of a 6-methyl group into coordinated pyridyl groups has substantial influence on the thermal stability of μ-peroxo diiron complexes. The order of thermal stability of oxy-**1**, -**2**, -**3**, and -**4** depends on the numbers of 6-methyl groups in the dinucleating ligands (Me_4-tpdp > Me_2-tpdp > tpdp). This order implies that the introduction of a 6-methyl group into the pyridyl group suppresses some deleterious, irreversible decay reactions of μ-peroxo diferric species. If the decay reaction proceeds via a higher valent iron species such as Fe(IV), the electron donor ability of the ligands seems to be important because the weaker electron donor would suppress the formation of an Fe(IV) species and facilitate the reformation of diferrous species from μ-peroxo diferric species. If the decay reaction is bimolecular, the steric properties of the ligand seem to be important because the bulkier ligand which can form a hydrophobic pocket surrounding the O_2-binding site would provide unfavorable interactions in the transition state of the decay reaction. In either case, a 6-methyl group would suppress the irreversible oxidation and facilitate the reversible oxygenation.

For the corresponding cobalt(II) complexes $[Co_2(L)(CH_3COO)]^+$, the 6-methyl group has a significant influence on the oxygen affinity. The tpdp complex forms a μ-peroxo complex ($P_{1/2}(O_2)$ = 760 Torr at −15.6 °C in acetonitrile),[25c] whereas the Me_2-tpdp complex (**5**) has no reactivity with O_2 even at −60 °C. Introduction of a 6-methyl group in the pyridyl group has been shown to cause a positive shift of the redox potential of various metal complexes, as pointed out by Hodgson et al.[32] and Que et al.[31] For instance, the $E_{1/2}$(II,III/II,II) and $E_{1/2}$(III,III/II,III) values of $[Fe_2(Me_4\text{-bpmp})(C_6H_5COO)_2]^+$ are 160−210 mV higher than those of $[Fe_2(bpmp)(C_6H_5COO)_2]^+$.[16a,41] Thus the electron donor ability of the 6-methylpyridyl nitrogen is weaker than that of pyridyl nitrogen, which stabilizes the lower oxidation state and appears to facilitate the reversible oxygenation. In addition, the electron donor ability of the bridging carboxylate is also responsible for the reversibility and oxygen affinity. The $E_{1/2}$(II,III/II,II) value of **2** is ca. 150 mV more positive than that of **1**, indicating that **2** prefers the iron(II) oxidation state compared to **1**. The thermal stability of **2** toward oxidation is greater than that of **1**, and the oxygen affinity of **2** ($P_{1/2}$ = ca. 41 Torr) is lower than that of **1** ($P_{1/2}$ = ca. 6 Torr) in CH_2Cl_2 at −40 °C.

The molecular structure of **1** shows a significant elongation of the Fe−N(pyridyl) bonds in the six-coordinate center relative to those in the five-coordinate center. If such an elongation of the Fe−N(pyridyl) bonds occurs in the oxy form associated with a change in the coordination number from five-coordinate to six-coordinate, this may also lead to a further weakening of the electron donor ability of the 6-methylpyridyl nitrogen. Such a dynamic stereochemical motion during the change in the oxidation state between iron(III) and iron(II) (oxygenation−deoxygenation process) might also prefer the iron(II) oxidation state and facilitate a reversible deoxygenation.

Que et al. reported that polar solvents such as DMSO greatly stabilize the μ-peroxo species (polar solvent effect). A similar polar solvent effect is also observed in the present complexes as mentioned above. However, coordination of DMSO to the five-coordinate iron center significantly decreases the oxygenation rate. The slow oxygenation in the presence of DMSO indicates that only the five-coordinate iron center can react with O_2. In the previous studies, we found that the dinuclear cobalt(II) and iron(II) complexes [Co_2- or $Fe_2(L)(RCOO)_2]^+$ (L represents the dinucleating ligands such as bpmp), which have two six-coordinate metal centers, are stable toward O_2, whereas the corresponding five-coordinate complexes $[M_2(L)(RCOO)]^{2+}$ are very reactive with O_2.[16a,25b]

Concluding Remarks

New dinuclear iron(II) complexes with alkoxide and carboxylate bridges, $[Fe_2(L)(RCOO)(H_2O)]^+$ (L = Me_4-tpdp, Me_2-tpdp, or tpdp), were synthesized and characterized. The Me_4-tpdp complexes have two distinct iron centers in the solid state: one five-coordinate iron center with an N_3O_2 donor set and one six-coordinate iron center with an N_3O_3 donor set having an additional coordinated water molecule. In CH_2Cl_2, however, a structural change occurs and gives rise to two five-coordinate iron centers. The complexes of Me_4-tpdp with two five-coordinate centers react with O_2 reversibly to form μ-peroxo complexes, which were characterized by UV−visible and Raman spectroscopies and oxygen affinity measurement. The thermal stability (reversibility) of the μ-peroxo diferric complexes is highly dependent on the relative degree of steric bulkiness and the electron donor ability of the ligands; the order of the thermal stability depending on the ligands is Me_4-tpdp > Me_2-tpdp > tpdp and CF_3COO^- > $C_6H_5COO^-$. Introduction of a 6-methyl group into the pyridyl group suppresses some deleterious, irreversible decay reactions of the μ-peroxo diferric species.

Acknowledgment. This work was partly supported by a Grant-in-Aid for Scientific Research on Priority Area (No. 03241105).

Supporting Information Available: Tables of fractional atomic coordinates, thermal parameters, and bond distances and angles for **1**, packing diagram of complex **1**, plot of $P(O_2)$ vs $P(O_2)/\Delta A$ for **1** and **2**, and ^1H NMR spectra of **2** in CD_2Cl_2 at 300 K and oxy-**2** in CD_2Cl_2 at 213 K (Figures S1−S3) (12 pages); listing of observed and calculated structure factors for complex **1** (19 pages). This material is contained in many libraries on microfiche, immediately follows this article in the microfilm version of the journal, can be ordered from the ACS, and can be downloaded from the Internet; see any current masthead page for ordering information and Internet access instructions.

JA943737V

(41) $[Fe_2(Me_4\text{-bpmp})(C_6H_5COO)_2]BF_4 \cdot H_2O$. Anal. Calcd for $C_{51}H_{53}N_6O_6Fe_2BF_4$: C, 58.65; H, 5.11; N, 8.05. Found: C, 58.61; H, 4.98; N, 8.05. $E_{1/2}$ values of Fe_2(II,III)/Fe_2(II,II) and Fe_2(III,III)/Fe_2(II,III) couples in CH_3CN are 190 and 920 mV vs SCE. (Suzuki, M.; Uehara, A. Unpublished data).